22
Medical Imaging (MRI Coils)

Dario Mager, Elmar Fischer, Andreas Peter, Patrick J. Smith, Jürgen Hennig, and Jan G. Korvink

22.1
Introduction to Medical Imaging

Knowledge of patient anatomy has always been the primary goal of physicians. However, until the discovery of X-rays by Wilhelm Conrad Röntgen in 1895 [1], the only way to get insight into a patient's body was by surgery. While Röntgen was working with an electrical discharge tube he discovered that a carbon board that he used to seal off the light from setup showed fluorescence, even though it was a few meters away from the setup. He performed a series of tests on the transparency of these new types of rays for various materials and found that the intensity of the rays was determined by the lightening effect on a photographic film. During these tests, he also took the first later-called *''röntgenogram''* when he placed his wife's hand on the photographic plate. With that work, Röntgen paved the way for a revolution in medical diagnosis. X-rays were used to get insight into the body nondestructively and have been used to detect bone fracture, ever since [2].

Not only by taking one X-ray image from one side but also by circling the X-ray source together with its sensor around a patient, a large number of X-ray images (= two-dimensional shadow casts) can be recorded. Reconstruction of three-dimensional space from these two-dimensional images is done in computed tomography, and analysis leads to full three-dimensional tissue information of the patient.

In contrast, X-ray-based methods have two main problems: First, they inflict quite a high dose of ionizing radiation on the patient, which can cause cancer, and second, this method is based on the absorption of the rays by tissues preferring massive atoms of high atomic number. Therefore, X-ray methods are mostly used for hard tissues such as bones that show strong absorption and good contrast.

A method for observation of soft biological tissue of low atomic number has emerged over the past decades and is known as magnetic resonance imaging (MRI). In addition to the possibility of giving three-dimensional insight into a patient's body, it is a noninvasive method, not penetrating the patient with ionizing radiation. The technique is based on the phenomenon of nuclear magnetic resonance (NMR).

22.2
Basics of Magnetic Resonance Imaging

MRI is based on the phenomenon of NMR, which was discovered in 1946 by Bloch and Purcell for atomic nuclei with a nonzero magnetic moment. To understand the principles, NMR is described first, then, the extension to MRI is made. A prerequisite for both phenomena is a superconducting magnet that provides a homogeneous magnetic field B_0 with a field strength usually exceeding 1 T.

NMR exploits the fact that physiologically important isotopes such as ^{1}H or ^{13}C have a nonzero nuclear magnetic moment. The existence of a nuclear magnetic moment is a quantum mechanical effect and has no classical explanation. Such nuclei with nonzero magnetic moment, when placed in a magnetic field of certain strength, will assume one of two states of different energy with the energy difference being linearly proportional to the B_0 field [3].

Thus, in thermal equilibrium, the number of nuclei in the higher energy state is slightly less than the number of nuclei in the lower energy state, leading to a net nuclear magnetization pointing in the direction of the magnetic field. Nuclei in the higher energy state can move to the lower energy state by emitting a photon, and nuclei in the lower energy state can also absorb a photon that matches the energy difference between the states and jump to the high energy state.

Therefore, photons of correct energy, which are actually electromagnetic fields of a certain frequency generated by a radio-frequency (RF) probe, can induce transitions in such a two-level system of the nuclei and destroy thermal equilibrium. Immediately after such a disturbance, relaxation back to equilibrium will take place and excess nuclei in nonequilibrium states will emit or absorb photons to recover equilibrium. Chemical bonds can cause an additional shift of the resonance frequency, thus, nuclei in different molecules are coded into the frequency domain.

The frequencies of emitted or absorbed electromagnetic signals reflect the presence of certain nuclei, and their relaxation back to thermal equilibrium is also affected by the molecular environment. Therefore, the NMR signal received by an RF probe has been widely used for many years to study spectroscopic properties of nuclei and their environment. The obtained information was already a huge improvement for biological and chemical analysis, and NMR has become one of the standard analysis techniques for chemists, allowing analysis of chemical structures and interactions. On the other hand, NMR only provides information about the abundance of elements inside a sample, not about their spatial distribution. Unlike in chemistry, a list of the components in a sample alone is not very useful for medical application. Only with an image that gives the spatial distributions of materials the method could make useful contributions to the medical field. In 1973, Lauterbur started to exploit the field strength dependency of the signal frequency by overlying the B_0-field with much smaller gradient fields. By doing so, he published the first two-dimensional spatially encoded NMR picture, the birth of MRI [4]. Thus, making the energy difference between nuclear energy states dependant on their spatial

position, that is, varying the magnetic field strength over space, points in an object can be encoded by their energy difference, that is, their resulting RF frequency. The gradient fields cause each position to see a slightly different magnetic field and therefore process at different frequencies. A frequency analysis of the received signal gives position-coded intensities. Different directions in x, y, and z are obtained by switching the gradients. An RF pulse only affects the nuclear moments if the frequency is close to the Larmor frequency; therefore, a magnetic field gradient in the Z-direction only causes spin-magnets in a certain slice to process. A switched gradient causes different precessing frequencies in the Y-direction and is measured evaluating the phase information. Local information created by the X-gradient is evaluated using the frequency shift [5] during signal acquisition. This imaging recovery process was developed based on work done by Mansfield [6, 7].

Hydrogen is the most important nucleus in medical analysis because of its presence in all biological tissue. In MRI, therefore, hydrogen protons ^{1}H are predominantly targeted. Their precessing frequency, the so-called Larmor frequency, f_0 is determined by the following equations:

$$f_0 = \frac{\omega_0}{2\pi} \tag{22.1}$$

$$\omega_0 = \gamma_x B_0 \tag{22.2}$$

γ_x, the gyromagnetic ratio, is a constant of material x that determines the angular velocity ω_0 of precession with regard to the magnetic field strength B_0 [8]. For hydrogen as the most prominent nucleus, $\gamma_H = 267.54$ MHz T^{-1}. The Larmor frequency of hydrogen scales linearly with the magnetic field strength.

$$f_0 = \frac{\gamma H}{2\pi} B_0 = \frac{267.54}{2\pi} B_0 = 42.58 \times B_0 \tag{22.3}$$

As only the sum of aligned spin-magnets, that is, the magnetization, contributes to the measurable signal, the higher the magnetic field, the higher is the amount of these spin-magnets and thus the magnetization. For this reason, magnetic field strength has been constantly increased to higher values. Modern NMR systems have field strengths up to 23.5 T, corresponding to a Larmor frequency of 1 GHz [9].

Considering magnetic energy, the aligned spin-magnets are at a low energy level. When disturbed from equilibrium by a strong RF pulse B_1 the macroscopic net magnetization M is tilted by an angle away from its equilibrium parallel to B_0 and starts to rotate (or precess) around B_1 after the RF pulse. In order to get back to equilibrium, spin-magnets have to decrease their energy level by emission or absorption of photons, that is, electromagnetic energy. A rotating magnetization and thus a time-varying magnetic field will induce a small voltage in a neighboring sensor coil, a signal that is called "free induction decay" (FID). The induction of a voltage and consequently, a current into a receiver circuit [10], is similar to a generator, in which a magnet induces a signal in a surrounding coil [11].

22.3
Resonant Receiver Circuit Theory

22.3.1
Receiving the RF Signal of the Spins

The signal should be picked up as close as possible to the signaling spins. The spin signal is triggered by the RF pulse sent out at a given frequency. Therefore, the receiving antenna needs to pick up a repetitive signal. Its frequency corresponds to the Larmor frequency of hydrogen of the scanner. The scanner used for the coils described in this chapter is a BioSpec 94/20 from Bruker (Bruker BioSpin GmbH, Germany). It has a $B_0 = 9.4$ T field and a 20 cm diameter bore (d_{bore}). For 9.4 T, using Eq. (22.3), the Larmor frequency is 400 MHz. This should be the central receiving frequency of the pickup coils. BioSpec has a gradient strength G_{xyz} of 0.44 T m^{-1}. Multiplying this value with the bore diameter and the gyromagnetic ratio gives Δf, the bandwidth of the signals created in the gradient field.

$$\Delta f = \pm \gamma H G_{xyz} \frac{d_{bore}}{2} = \pm 42.58 \left(\text{MHz T}^{-1} \right) \times 0.44 \left(\text{T m}^{-1} \right) \times 0.1 \text{ m}$$
$$= \pm 1.87 \text{ MHz} \tag{22.4}$$

The pickup coil should therefore show good receiving performance at 400 ± 2 MHz. The voltage U induced in a receiver coil by a precessing magnet follows Lenz's rule [12]:

$$U = -L \frac{dB}{dt} \tag{22.5}$$

As the change of magnetic flux caused by the precessing magnet is very small, the signal processing must be quite selective. The signal could be directly amplified, close to the receiver circuit, with a low-noise amplifier (LNA), but this would mean that all the electronics and supply cables need to go into the bore of the scanner. Another way is to do the amplification outside the bore and to transfer the signal to the amplifiers through a cable. To get as much of the signal from the receiver circuit to the amplifiers, a resonant receiver circuit is used.

22.3.2
The Components of a Resonant Receiver Coil Circuit

A resonant receiver circuit is a passive electronic circuit that consists of an inductor L and a capacitor C. Both capacitors and inductors can store potential energy. The capacitor stores the energy by shifting electrical charges into nonequilibrium positions, while an inductor stores the energy by building up a magnetic field. Owing to these phenomena, the two devices are complementary in their reaction to switching of a power supply. By combining C and L in one circuit, a second-order RLC resonant circuit is formed. The two components, C and L, determine the resonance frequency. These components have frequency-dependant resistive values, the reactances X_C and X_L, because of the storage principles of the devices. The

parasitic resistance will be neglected in this discussion, as the resistive part R only damps the resonance and thereby reduces the selectivity of the circuit, but has little influence on its center frequency. This resonance is caused by the complementary energy storage principles of L and C; the two keep pumping the energy into each other, while the resistive part damps the resonance. The system is not unstable, so it starts oscillating under a constant input signal. It only works if there is an input signal that continuously pumps energy into the circuit at the resonance frequency.

The reactances change inverse to each other with frequency, as described by the following formulas:

$$X_C = \frac{1}{2\pi Cf} \tag{22.6}$$

$$X_L = 2\pi Lf \tag{22.7}$$

A capacitor completely blocks a DC current ($X_C \to \infty$); on the other hand, for an infinitely high frequency, the capacitor behaves as a short circuit. An inductor shows the inverse behavior, having a high reactance X_L at high frequencies. By equalizing the reactances from Eqs. (22.6) and (22.7), the resonance frequency f_{LC} can be calculated as [13]

$$f_{LC} = \frac{1}{2\pi\sqrt{LC}} \tag{22.8}$$

The circuit works as a bandpass filter around f_{LC}. Therefore, f_{LC} should be equal to the spin resonance frequency f_0 to filter out ambient noise from the magnetic resonance (MR) signal. To keep the noise in the circuit to a minimum, the ohmic resistance in the circuit should be as low as possible. To transfer the signal to the scanner, a coaxial cable is used. The cable and the amplifier are matched to a characteristic impedance of 50 Ω. If the circuit is matched to 50 Ω, the signal is transferred without reflections and disturbances. *L* and *C* are chosen to give a frequency that is as close as possible to the spin frequency. For fine-tuning, external capacitors are added to the circuit to tune the circuit to the desired central frequency and to match it to 50 Ω [13]. A schematic representation of the complete circuit is shown in Figure 22.1.

22.3.3
The Printing of the Resonant RLC Structures

The key idea is to directly ink-jet print the complete RLC circuit [14]. This approach allows one to rapidly produce receiver circuits of a specific shape with high precision. Therefore, the notations R, L, and C are replaced by ink-jet-printed representations of the components [15]. Any loop-shaped conductor forms an inductor, with a value defined by its shape and the material surrounding the wire. The L is therefore defined by the shape and size of the wire loop. The wire in this case is an ink-jet-printed line of a metal containing ink. This track has a limited conductivity which defines the *R* of the circuit.
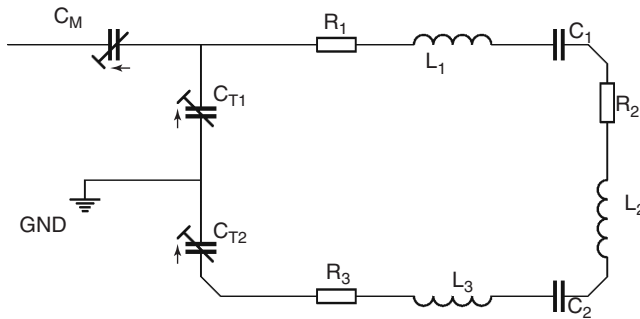
Figure 22.1 Schematic representation of an RLC circuit including tuning (C_{Tx}) and matching capacitors (C_M). The resistors (R_x) and the inductors (L_x) are the resulting physical properties of the ink-jet-printed tracks. The capacitors (C_x) are the track overlaps.

The Cs are created by printing parts of the conductive tracks on adjacent sides of a thin substrate. These two conductive areas are separated by a thin isolator (the substrate) and thus form a capacitor. All three components can, therefore, be created in a planar ink-jet printing process. The idea is to create an operational, planar surface receiver coil by ink-jet printing [16, 17].

22.3.3.1 The Ink-jet Printing of R and L

For the production of MRI receiver coils, silver tracks were printed onto a flexible Polyimide (Kapton) foil. The tracks of the coils define both values L and R, the L is given by the area surrounded by the track and the R by its thickness, length, and conductivity. Silver was chosen because of its high electrical conductivity (62×10^6 S m^{-1}) and Kapton for being flexible and stable at high temperatures ($\sim$400 °C). Flexible substrates are required because they allow the final coil to be bent around the samples. Although there are specialized printheads that allow the printing of molten solder at temperatures up to 500 °C [18, 19], silver cannot be printed in its molten state because its melting point is 962 °C. Even though there would be a printhead that could print liquids at these high temperatures, there would be no suitable flexible substrates available. Therefore, an ink containing silver nanopowder is used, which is easy to handle and stable to print at room temperature and gives a good conductivity if sintered for 5 min at 300 °C. The sintering temperature and time have a large influence on the conductivity. The higher the temperature, the shorter is the sintering time needed to reach a given conductivity [20]. At 300 °C, the ink reaches its final conductivity within minutes. The ink is nanoparticle ink sold under the name SunTronic U5603 by SunChemicals (Slough, GB). The formulation of ink allows straightforward printing with most commercial printheads.

For the coils presented, a Dimatix DMP-2831 Material Printer was used. The printer was equipped with a 10 pl printhead. The Kapton foil used had a thickness of 50 μm. The foil was used both as a substrate and as a dielectric. The printing

parameters, dot spacing, and printing speed were chosen to ensure the homogeneity of the deposited layers [21, 22]. All structures were printed with a dot spacing of 25 µm, which corresponds to a pixel density of 1016 dpi at a frequency of 5 kHz. Both printhead and substrate were maintained at room temperature.

The tracks were printed as multilayers. Two layers were printed; then the foil was sintered on a hot plate for 5 min at 300 °C. The next two layers were then printed on top and then again sintered. The operational coils had six or eight layers to have a good conductance. The tracks were sintered in between because pilling up six to eight layers leads to quite high contact angles, which tend to become unstable and destroy the homogeneous line shape.

At high frequencies the so-called skin effect causes a current to be conducted only at the rim of a wire. The penetration depth or skin depth δ in silver can be calculated using the following formula:

$$\delta = \sqrt{\frac{\rho_{silver}}{\pi f \mu_0 \mu_r}} = \sqrt{16 \times 10^{-9} \pi \times 4 \times 10^8 \times 4\pi \times 10^{-7} \times 1} = 3.2 \,\mu m \tag{22.9}$$

In this formula, μ_0 is the magnetic permeability and f is the frequency of the signal. The relative permeability μ_r needs to equal 1 because of the specially high-Tesla environment. Therefore, a track height of $2 \times 3.2 \,\mu m$ is enough to get the best possible conductivity at 400 MHz.

### 22.3.3.2 The Ink-Jet Printing of C

Capacitors are built of two conductive electrodes that are separated by an insulator. This principle is found in all forms of capacitors (even in so-called supercapacitors in which the insulator is just a thin electrochemical double layer). The shape of the electrodes is not that important. The crucial parameters are the area of the adjacent electrodes, the distance between them, and the value of the dielectric constant of the separating insulator. Therefore, most capacitors are built as plate capacitors. They are mostly not flat, but rolled up or stacked, to keep the final devices small.

Equation (22.10) describes the capacitance of an ideal parallel plate capacitor. This simplification is valid for most plate capacitors, as it neglects effects at the edges of the plates and is therefore valid as long as the area (side-length) of the electrodes is much larger than their distance from each other, which holds for nearly any planar capacitor.

$$C = \varepsilon_0 \varepsilon_r \frac{A_C}{d_C} \tag{22.10}$$

The permittivity $\varepsilon_0 = 8.8542 \times 10^{-12} \,F\,m^{-1}$ gives the resulting capacitance for a given geometry. ε_r weighs the general permittivity for the insulator material used. A_c is the area of the electrodes and d_c the thickness of the dielectric.

For the application of the MR receiver circuit, two capacitors with values in the low picofarad range are needed in the receiver, to reduce wavelength effects. Therefore, the approach for creating capacitors is introduced using the substrate as dielectric, as shown in Figure 22.2a,b. The conductive track of the inductive loop is cut open and placed on two sides of a thin dielectric substrate. At the position where the sides

(a)

(b)
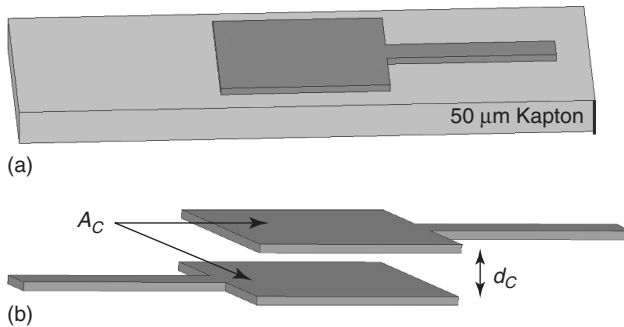
Figure 22.2 (a) Computer aided design (CAD) model of a plate capacitor printed on Kapton. (b) The model with the Kapton removed to get a better understanding of the arrangement.

are changed, these tracks overlap for a certain area. Owing to the thin substrate, the arrangement forms a capacitor according to Equation (22.10). The capacitance caused by adjacent tracks is normally a parasitic effect that should be kept small, but for this application and the production technique of inkjet printing, it was turned into a feature. But for this application and the production technique of ink-jet printing, it was turned into a feature. This is feasible only because of the small capacitive values needed for the targeted application. For ink-jet printing, this approach reduces the number of processing steps, as the dielectric does not need to be printed. Hence the capacitors can be directly produced, just using ink-jet printing and some mechanical handling, such as turning the substrate and placing it on the hot plate.

For the Kapton foil, the thickness ($d = 50\,\mu\text{m}$) and the dielectric constant ($\varepsilon_r = \sim 3.4$) are pretty much known. Therefore, the design of the capacitor becomes mainly a geometrical problem.

Nevertheless, for most materials, there is not an exact value for ε_r, because it differs depending on the exact composition of the material and the measured frequency.

Kapton is the ideal substrate for the application. It has a decent ε_r, comes in different thicknesses, is thermally stable to quite high temperatures, and is nonmagnetic.

A straightforward way to increase the capacitor value would be to use thinner foils. But the choice of substrate thickness is, beside the suitability for manual handling during production, also influenced by its ability to ensure a rigid placement during printing and of the final receiver circuit on the measurement sample. Therefore, $50\,\mu\text{m}$ thick Kapton gives a good compromise between mechanical stability and achievable capacitance if used as a dielectric.

Figure 22.3a gives an example of how the capacitor can be directly built on the top and bottom of the Kapton substrate. As the two parts of the loop need to be perfectly aligned, the transparency of Kapton is a helpful feature. Taking $50\,\mu\text{m}$ as the thickness and 3.4 as the dielectric constant Equation (22.10) gives the capacities
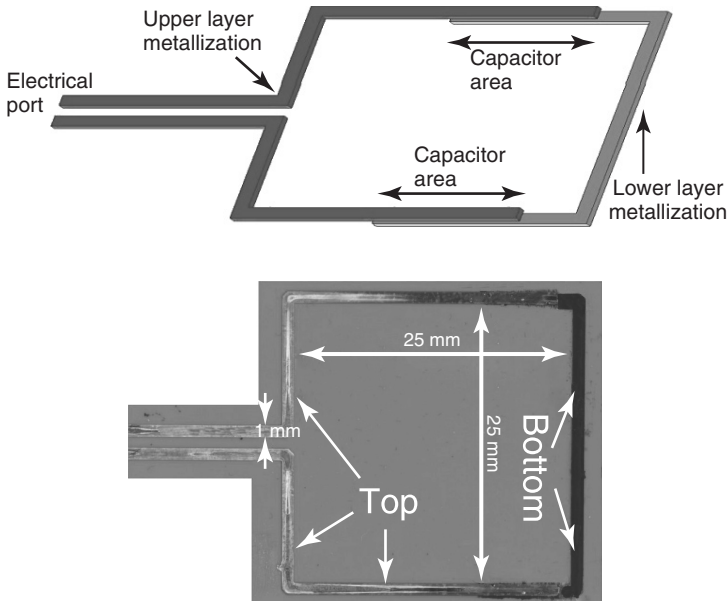
Figure 22.3 (a) Sketch of the complete circuit including the ink-jet-printed capacitors. (b) An image of the ink-jet-printed circuit.

per square millimeters that can be seen as an initial guess.

$$C_{\text{Kapton}} = \frac{\varepsilon_0 \varepsilon_r}{d_C} A_C = \frac{8.8542 \times 3.4}{50} 10^{-6} A_C = 0.602 \left(\text{pF mm}^{-2} \right) A_C \quad (22.11)$$

22.4
The Ink-Jet-Printed Resonant Circuit

As described in the previous section, the capacitor values cannot be perfectly predicted. Therefore, the matching to the 50 Ω of the measurement equipment and the resonance frequency are never perfectly obtained. The real matching is determined using a network analyzer by measuring the reflection coefficient at the resonance frequency f_{LC}. The value of R determines how selective the bandpass filter is. The selectivity is quantified by the bandwidth Δf_{LC} between the two frequencies, with a reflection coefficient S_{11} of −3 dB, indicated by the horizontal line in Figure 22.5.

Using bandwidth Δf_{LC} and the center frequency f_{LC}, a characteristic number, the so-called Q-factor can be calculated. The Q-factor allows different circuits to be compared. As stated before, the resistance has little influence on the central frequency. For the bandwidth, on the other hand, the influence is quite severe.

A higher bandwidth means that the circuit is less frequency selective and, therefore, receives more noise, and as the Q-factor gives the amplitude amplification quality of the circuit (the signal at f_{LC} is multiplied by Q[23]), the signal enhancement

is also reduced. Being built of passive components the circuit cannot really amplify a signal, but it can accumulate the repeatedly picked up signal, up to the point at which the signal level is so high that the energy dissipated by the resistive part equals the incoming inductive quantum per period. Using the values from Figure 22.5, Q is calculated as follows:

$$Q\text{-factor} = 2\frac{f_{LC}}{\Delta f_{RLC}} = 2\frac{400\ \text{MHz}}{26\ \text{MHz}} = \sim 30.8 \tag{22.12}$$

Using such a circuit, the signal amplitude is increased by a factor of $\sim$30 before it is transferred to the amplifier of the scanner [23, 24].

22.5
Imaging Using IJP Planar Surface Receiver Coils

The dimensions of the coils were given by the application in the MR scanner, because as a general rule, the depth of view of a coil is roughly the size of the coil's diameter. The inductance of a coil scales with its area and the permittivity properties μ_r of the surrounding materials. The materials close to the coil are given by the application; these materials all have an μ_r close to 1. Therefore, the main parameters for tuning the circuit to the desired frequency are the capacitors. The capacitors are used not only to tune the resonance frequency but also to help reduce wave effects in the coil by ''lumping'' the conductive track. The targeted depth of view is $\sim$25 mm. For the 25 mm square-shaped coil from Figure 22.3b, the perimeter is 100 mm. Adding the contacting tracks, which are used to connect the coil with the clamp holder, the whole track has a length of $\sim$120 mm. The wavelength at 400 MHz in the conductive loop was estimated to be $\sim$600 mm and thereby only five times longer than the geometrical length. The length of the conductor cannot be changed to ensure that the wavelength is between 10 and 20 times longer than the geometrical length. But the conductor can be cut into shorter pieces, which are connected by capacitors. This ''lumping,'' which interrupts the track for DC, does not account for high frequencies, as the capacitors bridge the gap, but they reduce the wave effects. The required components of a resonating RLC circuit for a frequency of 400 MHz can be obtained through circuit theory. As L and C contribute equally to the resonance frequency, theoretically, an infinite number of possible combinations are possible. However, for a balanced and feasible circuit, the useful values are limited to values achievable by the production process.

The shape and the dimensions were obtained using an ADS/Momentum (Agilent, Santa Clara, California) simulation. On the basis of these values, the receiver coil can be dimensioned and hence ink-jet printed. The structure of the coil is sketched in Figure 22.3a, and a photo is shown in Figure 22.3b. The coil consists of a fork-shaped top layer and a ''U''-shaped bottom layer. The ''fork'' and the ''U'' overlap at two points; these overlaps form the capacitors. Figure 22.3b shows the top view of an ink-jet-printed coil; the tracks have a width of 1 mm and a thickness of $\sim$3 μm. The top side tracks are reflecting the light and are therefore brighter

than the bottom side ''U''-shaped track that is visible through the Kapton. Three parts were printed. Two parts were printed on top of the substrate, and one part was printed on the bottom of the substrate. The centers of the two 1 mm wide track ends are 2 mm apart, thereby fitting into a standard clamp holder and having a small inductance. The active main area for the inductance is a 25×25 mm^2.

22.5.1
Tuning and Matching of the Circuit

Using the two track ends on the left side of Figure 22.3b, the loop is connected via a clamp connector to a small printed circuit board (PCB) that contains the tuning and matching capacitors and a high-frequency SMA plug to connect the circuit to the measurement equipment. To evaluate the quality of the ink-jet-printed circuits, they were electrically characterized using an Agilent 5071C network analyzer. The complete circuit including the tuning and matching capacitors and the cable connector is shown in Figure 22.4.
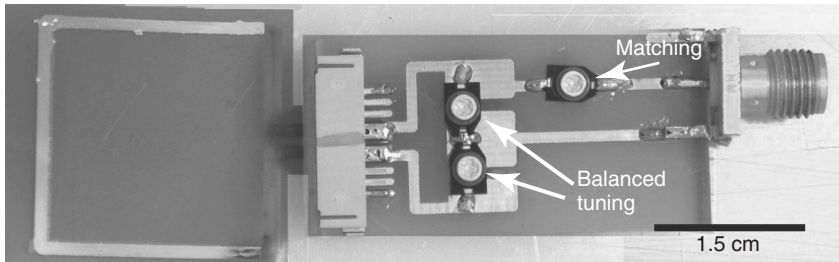
Figure 22.4 The receiver circuit mounted into the tuning and matching PCB.
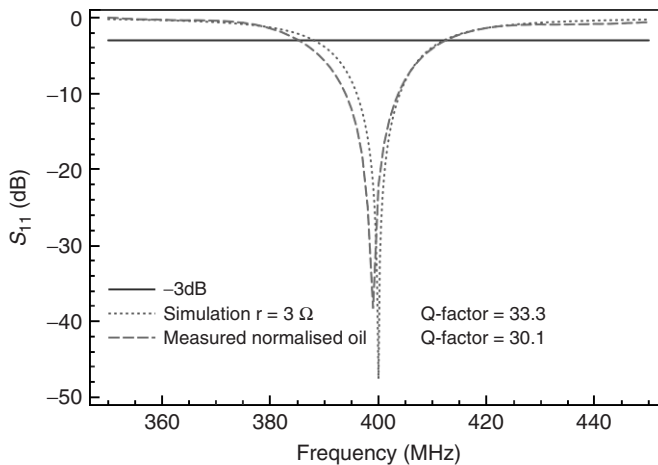
Figure 22.5 Frequency response of the circuit, a simulation, and a measurement are plotted.

The frequency response of the tuned and matched circuit is shown in Figure 22.5. The plot shows the frequency-dependent reflection response of the circuit, the so-called S_{11} parameter. Beside the measured curve of the ink-jet-printed circuit, a simulated circuit is given. The similar shapes of the curves indicate that the simulated circuit represents the real one quite accurately.

The Q-factor of ∼30 is far from being an outstanding value, but they still increase the received signal quality considerably. The signal can be improved further by improving the flatness of the tracks to get a better conductivity in the rim. The following section underlines this argument by taking MR pictures using the ink-jet-printed receiver circuit and comparing the results with those of standard receivers.

22.5.2
Magnetic Resonance Images

The final test for any receiver coil is its actual use in an MR scanner; the quality of the received image giving a good estimation of the coil's quality. Therefore, the ink-jet printing (IJP) circuit was used to record MR images with the earlier described Bruker BioSpec 94/20 scanner.

Surface coils were created for reception only, therefore, a commercial transmission coil (Bruker linear resonator, $d_i = 72$ mm) was placed in the central region of the 20 cm bore of the Bruker system for homogeneous excitation of transverse magnetization. Inside that coil, the ink-jet-printed receiver coil was mounted on the sample, which was a bottle of silicon oil, a standard reference material. Experiments have been performed in the so-called cross-coil mode, in which the actively decoupled linear resonator has been used to excite homogeneous transverse magnetization inside its sensitive volume, whereas the interesting receiver coil was used for reception in that volume. Signals recorded with the receiver coil in such an experiment therefore provide a sensitivity profile of that receiver coil because excitation is homogeneous over space around the coil and the recorded image represents the sensitivity of the coil for a constant excitation signal. Corresponding images were recorded using a fast low-angle-shot (FLASH) gradient echo sequence provided by the scanner software with identical image parameters ($T_R = 100$ ms, $T_E = 6.0$ ms, flip angle $= 30°$, slice thickness $= 2$ mm) for both coil types.

T_R is the repetition time of the experiment and denotes the time needed to reestablish thermal equilibrium. In case of the FLASH sequence [25, 26], equilibrium magnetization is tilted by a small flip angle of $30°$ only, therefore, disturbance of equilibrium is small and the pulse sequence can be repeated much faster than with flip angles of $90°$. The echo time T_E gives information on the duration of gradient pulses and reflects the time for which the recorded echo signal is attenuated by transverse relaxation including frequency offsets. In case of long T_E, one speaks of a T_2-weighted image, whereas attenuation by transverse relaxation can be neglected for the chosen $T_E = 6$ ms, only. Thus, mainly information on nuclear spin density is obtained. In theory and for ideal reception, all excited signals should be recorded, and for homogeneous excitation, one should observe
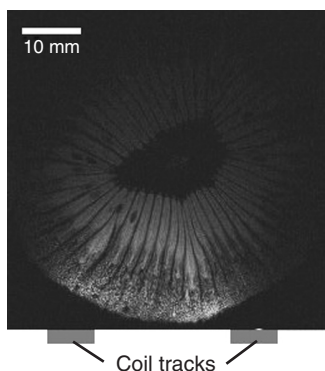
Figure 22.6 Image of a Kiwi fruit, taken with an ink-jet-printed receiver circuit. The models of the track are placed there to give a better understanding of the sensitivity gradient in the image.

constant signal not depending on space. In reality, reception depends on position and especially on the distance from coil wires of the receiver coils and therefore directly reflects the sensitivity profile of the receiver coil. Figure 22.6 shows images of a kiwi fruit taken by the Bruker system. The tracks of the coil were added as sketch to the image to illustrate the effect of the sensitivity gradient, with increasing distance to the receiving coil.

22.6
Summary

The approach of using ink-jet-printed conductive tracks, capacitors, and planar inductances to form an ink-jet-printed resonance circuit has been successfully demonstrated. The printed lines are highly conductive, so that the attenuation they cause does not significantly disturb the resonant circuit. Printing planar capacitors, using the substrate as dielectric, could be realized. Therefore, the created resonance circuit shows behavior comparable to standard PCB circuits with soldered discrete components.

Ink-jet-printed resonant circuits have been tested under all criteria relevant for MRI receiver coils. The process allows one, within certain limits, to create arbitrary-shaped 2D coils that show good receiving properties.

References

1. Röntgen, W.C. (1898) Ueber eine neue Art von Strahlen. *Ann. Phys. Chem.*, **64**, (1). 1–11.
2. Komitee (1901) Nobel Wilhelm Conrad Röntgen – Biography, *http://nobelprize.org/nobel_prizes/physics/laureates/1901/rontgen.html* (accessed 21 July 2010).
3. Doessel, O. (1999) *Bildgebende Verfahren in der Medizin: Von der Technik zur medizinischen. Anwendung*, Springer.
4. Lauterbur, P.C. (1973) Image formation by induced local interactions: examples employing nuclear magnetic resonance. *Nature*, **242**, 190–191.
5. Weishaupt, D., Koechli, V., and Marincek, B. (2009) *Wie funktioniert MRI?* Springer.
6. Mansfield, P. and Grannell, P.K. (1973) NMR 'diffraction' in solids? *J. Phys. C: Solid State Phys.*, **6**, L422–L426.

7. Mansfield, P. (1977) Multi-planar image formation using NMR spin echoes. *J. Phys. C: Solid State Phys.*, **10**, 55–58.

8. Vlaardingerbroek, M.T. and Boer, J.A. (2003) *Magnetic Resonance Imaging – Theory and Practice*, Springer.

9. Bruker (2010) 1GHz Scanner, *http://www.bruker.com* (accessed 23 February 2010).

10. Bloch, F., Hansen, W., and Packard, M. (1946) The nuclear induction experiment. *Phys. Rev. (APS)*, **70**, 474–485.

11. Faraday, M. (1832) Experimental researches in electricity. *Philos. Trans. R. Soc. Lond.*, **122**, 125–162.

12. Lenz, E. (1834) *Annalen der Physik und Chemie - Zweite Reihe*, J. C. Poggendorffs Verlag J. A. Barth, Heraus.

13. Tietze, U. and Schenk, C. (1999) *Halbleiterschaltungstechnik*, Springer.

14. Mager, D. *et al.* (2008) Can inkjet printing make MRI coils? The 16th Scientific Meeting of ISMR, Toronto.

15. Mager, D. *et al.* (2008) Inkjet printing of structures for MRI coils Digital Fabrication 2008, Pittsburgh, pp. 891–894.

16. Mager, D. *et al.* (2010) An MRI receiver coil produced by inkjet printing directly on to a flexible substrate. *IEEE Trans. Med. Imaging*, **29**, 482–487.

17. Mager, D. *et al.* (2009) Operational inkjet printed metal-on-kapton MRI receiver coil. 17th ISMRM, Honolulu.

18. Kessling, O. *et al.* (2008) An electro-magnetic actuator for printing solder. ACTUATOR 2008, 11th International Conference on New Actuators.

19. Metz, T. *et al.* (2009) StarJet: pneumatic dispensing of nano- to picoliter droplets of liquid metal. Proceedings IEEE-MEMS, Sorrento, Italy, pp. 43–46.

20. Dearden, A.L. *et al.* (2005) A low curing temperature ink for use in ink-jet printing and subsequent production of conductive tracks. *Macromol. Rapid Commun.*, **26** (4), 315–318.

21. Smith, P.J. *et al.* (2006) Direct ink-jet printing and low temperature conversion of conductive silver patterns. *J. Mater. Sci.*, **1**, 1–6.

22. Soltman, D. and Subramanian, V. (2008) Inkjet-printed line morphologies and temperature control of the coffee ring effect. *Langmuir*, **24**, 2224–2231.

23. Terman, F.E. (1950) *Radio Engineers Handbook*, Mc Graw-Hill.

24. Hoult, D.I. (1978) The NMR receiver: a description and analysis of design. *Prog. NMR Spectr.*, **12**, 44–77.

25. Haase, A. *et al.* (1986) FLASH imaging: rapid NMR imaging using low flip angle pulses. *J. Magn. Reson.*, **67**, 258–266.

26. Haase, A. (1994) Principles and applications of FLASH NMR imaging. *MAGMA*, **2**, 157–160.